DESIGN OF A NON-CONTACT VERTICAL TRANSITION FOR A 3D MM-WAVE MULTI-CHIP MODULE BASED ON SHIELDED MEMBRANE SUPPORTED INTERCONNECTS

N. E. S. Farrington[1, *] and S. Iezekiel[2]

[1]e2v Microwave Technology Centre, 168 Sadler Road, Lincoln, United Kingdom

[2]Department of Electrical and Computer Engineering, University of Cyprus, Nicosia, Cyprus

Abstract—The preliminary design concept, for a low-loss, high-bandwidth electromagnetically coupled vertical transition for use as a via between adjacent levels of a 3D-MCM based on membrane-supported striplines with micro-machined shielding, is presented. The design methodology, modeling using Ansoft HFSS and simulated results are presented and together represent a complete electrical characterization of the vertical transition. The simulated insertion loss of these structures is shown to be as low as 0.12 dB at 60 GHz with a 44 GHz 1 dB bandwidth. Besides studying the vertical transition, the analysis is extended to identify the range of directional coupling which can be achieved using this type of structure, which is shown to be greater than 3 dB. The structures studied rely on a versatile micromachining technique for the fabrication of the micro-shielding which allows for the conformal packaging of lines and devices, with the ultimate aim of realizing 3D system-in-a-package type modules. The concept and proposed fabrication techniques for these modules, including methods of flip-chip MMIC attachment are detailed.

1. INTRODUCTION

The advantages of membrane-supported lines and passive components for millimeter-wave frequencies include extremely low-loss and dispersion [1, 2] along with the potential for high-performance passives such as inductors, capacitors [3], directional couplers [4] and antenna

* Corresponding author: Novak E. S. Farrington (novak.farrington@e2v.com).

arrays [5]. The origins for this type of transmission line lie in a combination of the work conducted using a membrane-supported CPW (coplanar-waveguide) geometry on a $SiO_2/Si_3N_4/SiO_2$ membrane [3–8] (also demonstrated using a polymer or epoxy membrane [9–11]), and also that involving a self-packaged, grounded CPW (GCPW) configuration using micromachined silicon [12–17]. The work described in [1, 2] is an extension of these earlier types of miniature membrane-supported transmission lines with the addition of full shielding and conversion to a stripline-type geometry. This involved the use of a versatile photo-epoxy, SU-8 [18–22] for the fabrication of both the shielding and the membrane, which has already been proven in micromachining applications. This fabrication method involves the stacking of photolithographically defined thick layers to create complex 3D shielding configurations, as described in [22].

Micromachined silicon platforms have some benefits over polymer and epoxy technologies including process maturity, generally higher chemical resistance and thinner membranes. However, the level of geometrical complexity of the shielding structures which can be micromachined using polymers and epoxies is higher. This gives increased flexibility and scope which can be exploited to provide a platform with increased versatility. Compared to their silicon counterparts, SU-8 membranes display increased sturdiness and their processing supports the ability to remove areas of the membrane which are not mechanically important in order to gain electrical performance advantages. The increased versatility and relative ease of processing obtained through the use of this alternative micromachining approach for the shielding also affords certain major advantages. These include 1) the potential creation of novel electromagnetically coupled vertical transitions between shielded membrane-supported lines, which in addition can be adapted easily to provide varying degrees of directional coupling between the different levels of a MCM, and 2) support of methods for the attachment of MMICs directly to the membrane using conductive polymer flip-chipping. This would be extremely challenging on a silicon membrane due to the forces involved during the processing and assembly stages, and their inflexible processing sequence. This potentially makes the approach to line fabrication and assembly described in [1] a realizing technology for 3D MCMs using membrane-supported interconnects.

This paper describes the design, modeling and characterization of a non-contact vertical transition suitable for use in a 3D MCM employing the membrane supported transmission line interconnects developed in [1]. The results show that for an optimized 60 GHz transition, insertion losses of less than 1 dB over a 28 GHz bandwidth

should be possible. Further analysis has also shown that through the use of the membrane material removal technique described in [1, 2] this bandwidth could be increased to around 44 GHz.

2. MICROMACHINED MILLIMETER-WAVE 3D MCMS

The general motivation behind the development of 3D multi-chip modules is the miniaturization of microwave and mm-wave circuits. MCM technology mounts multiple unpackaged MMICs (monolithic microwave integrated circuits) or other active devices on a single substrate thereby combining more electronic functions in one module and so potentially reducing the physical size, cost and overall system complexity. In addition, individual chip-complexity can be decreased and so design flexibility increased through the use of application specific modular chip-sets (allowing the use of different material systems for different functions) and high-Q 'off-chip' passive components.

Extension to the third-dimension is possible using some of the micromachined millimeter-wave lines reviewed in [1] and this is demonstrated in the micromachined silicon 3D MCM proposed in [17, 23, 24] and detailed in Figure 1. This would use conventional via
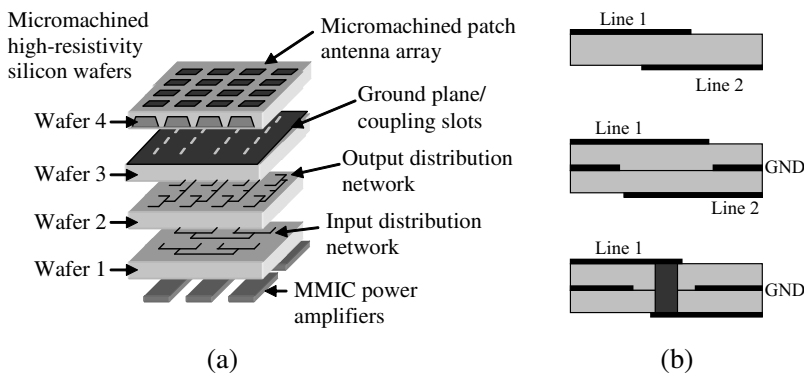

(a)   (b)

Figure 1. (a) Conceptual diagram of a highly integrated micromachined 3D MCM using conformal packaging and direct contact vertical transitions (after [23]), and (b) Cross-sections of vertical transitions (top to bottom): electromagnetically coupled microstrip or CPW transition through a common substrate [30], electromagnetically coupled microstrip transition through a common ground plane [28], and direct contact microstrip (or CPW) transition through a common ground plane [31].

formation between lines supported on bulk substrates and so require a transition between the membrane and bulk substrate supported lines. This potentially enables a system on a package (SoP) level of integration for a communication, radar or sensing system front end where the required MMICs, distribution networks and antenna array are all integrated into the same module.

2.1. Vertical Interconnects

The enabling component for the realization of 3D MCMs is a low-loss, high-bandwidth via to act as a vertical transition between lines on different levels of the module. The high-performance vias which have been extensively demonstrated so far fall into two categories: electromagnetically coupled [25–31] with at best, 0.2 dB insertion loss at W-band [30] for a microstrip type geometry, and direct contact transitions [31–35] with around 0.6 dB insertion loss at 94 GHz [31] for a coplanar line. Both of these have been demonstrated only between lines fabricated on bulk dielectrics. It should be noted here that although they exhibit a higher loss at mm-wave frequencies, direct contact transitions take up less space. It is noted here that microstrip to rectangular waveguide coupling structures, usually relying on a microstrip probe, have been successfully applied to the contactless connection between a plastic QFN package and rectangular waveguide at 77 GHz [36]. This technique has also been extended to coupling planar lines through an electrically thick ground plane to form a vertical transition in a 3D low temperature co-fired ceramic (LTCC) MCM at 40 GHz [37]. In the case of direct contact transitions (Figure 1(b)), application to membrane-based lines, due to their geometry and the required process sequence, would prove to be extremely problematic.

The electromagnetically coupled variety of vertical transitions have not, to the best of our knowledge, been demonstrated for membrane-supported lines because depending on line geometry, the separation between the strip conductors and the ground planes needs to be increased in the vicinity of the coupling region in order to achieve sufficient field interaction between the lines (this is demonstrated in Section 3.1). Since both upper and lower shielding would generally be required for each line in a 3D membrane-based MCM, this local variation in ground plane separation would be difficult to achieve using traditional fabrication techniques such as silicon micromachining. This means that their demonstration to date has only involved the coupling of unshielded coplanar lines with a common substrate [27, 30], or microstrip lines with a common substrate [30] or ground plane [25, 26, 28, 29, 31] (Figure 1(b)), and this has until now
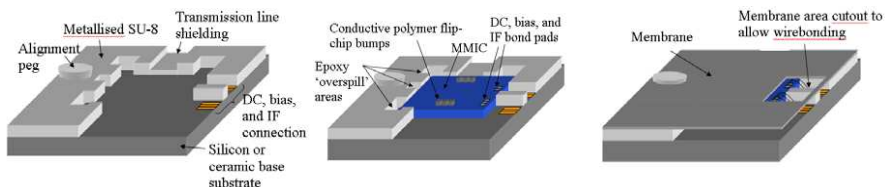
Figure 2. Proposed MMIC and active device attachment scheme (after [2]).

effectively eliminated membrane supported lines as an option for 3D MCMs. The electromagnetically coupled transitions discussed above fall into two main categories: capacitively coupled (Figure 1(b): first two diagrams) using overlaid quarter-wavelength lines, and inductively coupled using a narrow slot in the ground plane between overlaid lines.

The proposed 3D millimeter-wave MCM is similar in concept to that illustrated in Figure 1 but is fully compatible with the micromachined lines demonstrated in [1] and the vias characterized in Sections 3.1 and 3.2. The characterized vertical coupling structures allow the routing of millimeter-wave signals between the adjacent levels of a 3D module created by stacking self-aligning micromachined shielding and membrane layers. This fabrication technique would also potentially allow for the attachment of MMICs directly onto the membranes via a flip-chip technique [2, 38], which relies on a low-cost, lead-free, fluxless flip-chip technology based on the use of conductive polymers [38–43]. As shown in Figure 2, this would enable the back-side of the MMIC to be attached to a thermally conductive base-substrate while the high-frequency electrical connections are made directly to the membrane supported transmission lines. It is noted here that for the MCM concept and application illustrated in Figure 1(a) and described in [23], the MMICs or other active devices would be mounted on the base substrate and only the high-frequency distribution lines and passive components realized on the membrane itself: this means that no DC electrical connections would be required between membrane layers themselves.

3. DESIGN OF A NOVEL NON-CONTACT VERTICAL INTERCONNECT

The main difference between the coupled structures investigated here and those previously published is the use of a fully shielded stripline-type geometry [1] as opposed to microstrip. This complicates matters through the introduction of the extra ground planes and side shielding

for each line which will reduce coupling due to the increased signal-to-ground capacitance: this is highlighted in Figure 3. Here it can be seen that C_{12} represents the capacitance of the two strip conductors in the absence of a ground plane, while C_{11} and C_{22} represent the capacitance of each strip conductor and ground [44]. When the structure is symmetrical then $C_{11} = C_{22}$. For even mode excitation, C_{12} is effectively open-circuited meaning the even-mode capacitance and characteristic impedance are given by

$$C_e = C_{11} = C_{22} \tag{1}$$

$$Z_{oe} = \sqrt{\frac{L}{C_e}} = \frac{\sqrt{LC_e}}{C_e} = \frac{1}{vC_e} \tag{2}$$

where v denotes the propagation velocity on the line. It should be noted here that C_{11} (and C_{22}) will be slightly different for even- and odd-mode excitations due to the different charge distribution on the strip conductors for each case.

In the case of odd-mode excitation, the capacitance between either strip conductor and ground, and odd mode characteristic impedance are given by

$$C_o = C_{11} + 2C_{12} = C_{22} + 2C_{12} \tag{3}$$

$$Z_{oo} = \frac{1}{vC_o}. \tag{4}$$

This shows that due to the close proximity of the ground planes in comparison to the separation of the strip conductors, the effects of C_{11} and C_{22} will dominate the value of C_o and therefore Z_{oo}. This will also lower the range of practical values Z_{oe} may take.

For a directional coupler, the effects of the limitations placed on the values of Z_{oo} and Z_{oe} through the comparatively close proximity of the ground planes would be a reduction in the possible coupling between the two lines. This is shown by the relationship between the
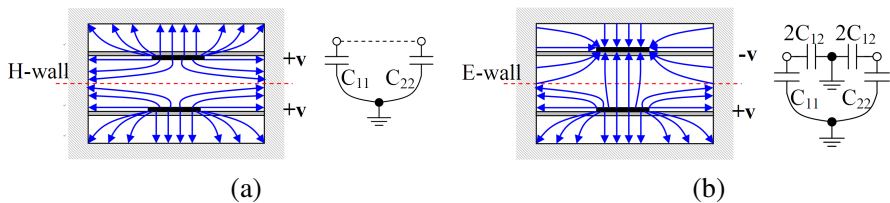

(a)   (b)

Figure 3. (a) Even-mode, and (b) odd-mode electric field pattern and equivalent capacitance network (After [44]).
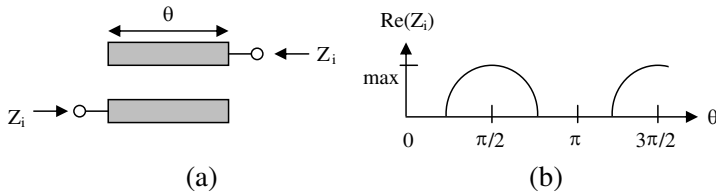
Figure 4. (a) Schematic representation of the vertical transition, (b) response of the vertical transition. (After [45].)

coupling factor, C, and Z_{oo} and Z_{oe} which can be described as [44],

$$C = \frac{Z_{oe} - Z_{oo}}{Z_{oe} + Z_{oo}} \qquad (5)$$

where the coupling factor C, is defined as the voltage coupling coefficient V_3/V.

In the case of the vertical transition, which is shown in schematic form in Figure 4(a), the optimum coupling will occur when the image impedance of the coupling structure is equal to the characteristic impedance of the input and output lines, with an effective coupling region length of $\lambda/4$ at the frequency of interest (Figure 4(b)). The image impedances, Z_{i1} and Z_{i2} for a two port circuit are defined as follows [45]: Z_{i1} is the input impedance at port 1 when port 2 is terminated with Z_{i2}, with Z_{i2} in turn being the input impedance at port 2 when port one is terminated with Z_{i1}. This means both ports are matched when terminated in their image impedances which in the case of a symmetrical vertical transition is

$$Z_i = \frac{\sqrt{(Z_{oe} - Z_{oo})^2 - (Z_{oe} + Z_{oo})^2 \cos^2 \theta}}{2 \sin \theta}. \qquad (6)$$

When the coupled line section is $\lambda/4$ long ($\theta = \pi/2$), this reduces to

$$Z_i = \frac{Z_{oe} - Z_{oo}}{2}. \qquad (7)$$

This shows that achieving optimum coupling is dependent on obtaining the values of Z_{oe} and Z_{oo} which meet the required image impedance condition.

3.1. EM Modeling and Characterization of the Coupled Line Structure

In order to establish the range of Z_{oo} and Z_{oe} possible for various practical geometries, a model of the structure was developed in Ansoft

HFSS. Using the parametric sweep function, several of the geometrical parameters were set up as variables as detailed in Figure 5(a), and the structures simulated using a full modal solution. The only parameters which were fixed were the strip conductor thickness, membrane thickness (1 μm and 10 μm respectively), and the separation S, of the two membranes. The separation was fixed at 260 μm to represent the distance between the vertically adjacent strip conductors
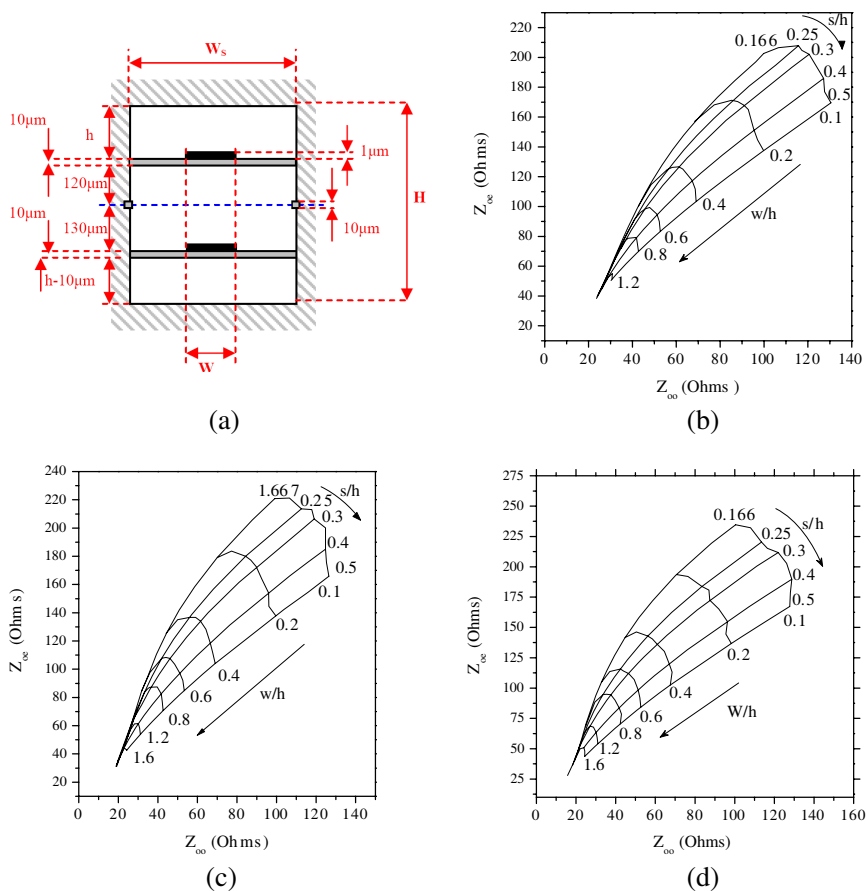

(a)

(b)

(c)

(d)

Figure 5. (a) Schematic cross-sectional (in the direction of propagation) representation of the coupling structure HFSS model and the geometrical parameters used, and normalized even- and odd-mode characteristic impedance design data at 60 GHz with (b) $W_S = 1000$ μm, (c) $W_S = 1250$ μm, and (d) $W_S = 1500$ μm.

of two stacked lines separated with a 10 μm thick metallized membrane acting as a common ground plane. It is noted here that the nominal line geometry was described in [1] and is such that the shielding side walls are 1000 μm apart, and the distance between the upper and lower shielding is 250 μm.

Due to the stacked nature of the transition's construction, the structure would in reality not be perfectly symmetrical. The slight asymmetry stems from that of the individual shielded lines themselves, along with the stacking of both membranes with the metallization on their upper surfaces. To obtain perfect symmetry in the structure, the upper or lower line (and therefore membrane) could be inverted. However it can be argued that the asymmetry would be a possible requirement in a 3D MCM, as bond wires may be needed to allow DC connections between the various levels. For this reason the asymmetry was included in the model.

The other variables were therefore the stripwidth W, the shielding width, W_S, and the total shielding height H (varied through an increase in the distance between the membranes and the upper and lower shielding, h). The transition shielding variables W_S and H were allowed to exceed those of the individual lines to mitigate the effects of the close proximity of the ground planes in relation to the strip separation. This would not present problems from a fabrication viewpoint if restricted to sensible limits. The limits imposed on the variables during the modeling were a maximum of W_S=1500 μm and $H = 1500$ μm for the shielding with the minimum matching those of the shielded lines. The maximum strip width, W was set to be 100 μm less than the value of W_S and the minimum set to 100 μm.

In order to obtain meaningful results the variables were swept in such a way that S, W and H could be normalised to give S/H and W/H for various values of W_S, allowing graphical representation of the results in the format of Z_{oo} versus Z_{oe}. The resulting data was manipulated to provide the design data plotted in Figures 5(b)–(d).

For each value of W_S, the effects of varying W and H are clearly seen and can be accounted for by referral to Eqs. (1)–(4). Decreasing W for a fixed H leads to an increase in both even- and odd-mode characteristic impedance due to a decrease in both $C_{11}(= C_{22})$ and C_{12}, as can be seen from the S/H curves on the plots.

The effects of increasing H for a fixed value of W/H will be an increase in C_{12} and an initial decrease in C_{11} ($= C_{22}$) as the separation between the strip conductors and the upper and lower ground planes increases. However, as W increases (to maintain the W/H ratio), so does its proximity to the side shielding, leading to an increase in C_{11}. The effect of this on Z_{oe} and Z_{oo} will be as follows: the change in C_{11}

due to increasing H, will lead to first an increase and then, if affected
by proximity to the side shielding, decrease of Z_{oe}. If the increase in
C_{12} is greater than the decrease in C_{11}, Z_{oo} will decrease in value (it can
be seen from the plots that this is generally the case) with increasing
H.

The main effect of increasing W_S is seen to be an increase in the
Z_{oe}/Z_{oo} ratio especially for large H where the range of possible Z_{oe}
values is significantly extended. This can be attributed to the reduced
values of C_{11} as the effect of the side shielding is reduced. The values
of Z_{oo} are not significantly altered by the increase in W_S.

The design data given in Figure 7 was also translated using Eq. (7)
to obtain the possible ranges of image impedance for a $\lambda/4$ long
coupling structure and this is illustrated in Figure 6. This confirms
that optimum coupling can be achieved for the transition and gives an
indication of the required geometry: with $W_S = 1500\,\mu m$, the ground
plane separation would need to be extended to $1000\,\mu m$.

The design data from Figure 5 was also used with Eq. (5) to
establish the coupling which could be achieved using a $\lambda/4$ line section
in a $50\,\Omega$ system. The results are shown in Figure 6(b) for a line with
$W_S = 1500\,\mu m$ which shows that greater than $3\,dB$ coupling could
be achieved when $H = 1500\,\mu m$. The results also suggest that $3\,dB$
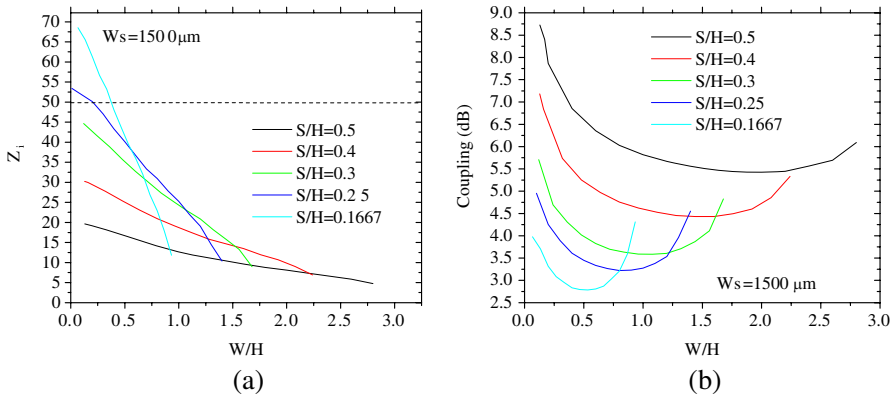coupling could be achieved with $H = 1000\,\mu m$ if W_S is increased.

Figure 6. (a) Image impedance plot for a $\lambda/4$ coupled line structure
with $W_S = 1500\,\mu m$, and (b) coupling for a $\lambda/4$ line section in a $50\,\Omega$
system: with $W_S = 1500\,\mu m$.

3.2. Design, Modeling and Simulation of the Vertical Transition

To design a vertical transition for fabrication, sensible limits on the geometry need to be imposed so as to reflect the requirements of a practical situation. This mainly concerns the assignment of a maximum value for H which was decided to be 1000 μm. At $H = 1000$ μm, the coupling structure's upper and lower ground planes could be incorporated into the metallization of the vertically adjacent lines in unused areas of the MCM as shown in Figure 7(a). In the illustrated structure the total height of the coupling region would be 1030 μm due to the inclusion of metallized membranes acting as the ground planes separating the lines.

The length of this region L_E, which is the distance from the end of the strip conductor to the end of the line shielding, was chosen to be twice that of the individual line height to minimise any effects on the coupling, and so was set in this case at 500 μm.

With the distance between the top and bottom shielding of the structure chosen to be $H = 1000$ μm, a value of $W_S = 1500$ μm was decided upon in order to easily achieve optimum coupling. Using Figure 6(a) and a small range parametric sweep in HFSS, the required conductor strip width was found to be $W = 260$ μm giving rise to the even- and odd-mode line characteristics listed in Figure 7(b). The initial length of the coupling region was taken to be a quarter of the geometrical average of the even- and odd mode wavelengths, and so L is set to 1185 μm to give a centre frequency, $f_c = 60$ GHz.

A model of the vertical transition coupling structure was

Parameter	Even-mode	Odd-mode
Characteristic impedance	202.5 Ω	101.4 Ω
Effective relative permittivity (ε_{reff})	1.114	1.1077
Wavelength (λ)	4.734 mm	4.747 mm
Propagation coefficient (β)	1327.2 rad/m	1323.5 rad/m

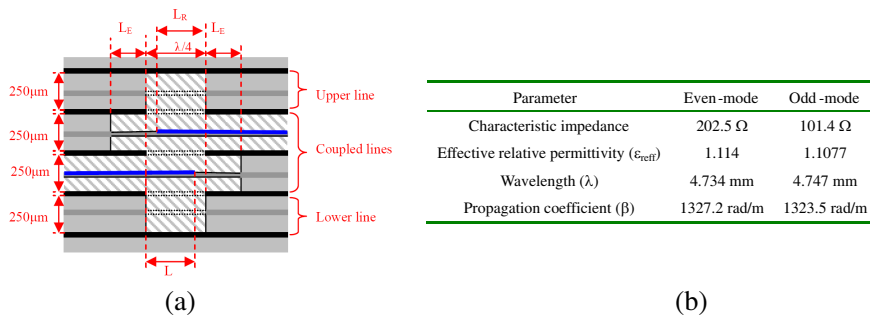(a)   (b)

Figure 7. (a) Integration of the vertical transition coupling structure into a membrane based 3D MCM, and (b) even-mode and odd-mode line characteristics for coupled lines at 50 GHz ($H = 1000$ μm, $W_S = 1500$ μm, $S = 260$ μm and $W = 260$ μm).

implemented in HFSS with 2 mm long feed lines, the effects of which were later de-embedded, is shown in Figure 8. Initially all materials included in the simulation were set as lossless to decrease simulation time while investigating the structure's frequency response. The results of the initial simulation are shown in Figure 9 which shows the centre frequency for the coupler with $L = 1185\,\mu$m to be $f_C = 50$ GHz. This deviation from the designed centre frequency is due to the fringing fields at the ends of the strip conductor effectively increasing the electrical length of the line. In order to compensate, the line was reduced to a length L_R while the shielding and gap in the common ground plane were left at their original length. As seen in Figure 9(a), a reduced line length of $L_R = 1035\,\mu$m resulted in the desired centre
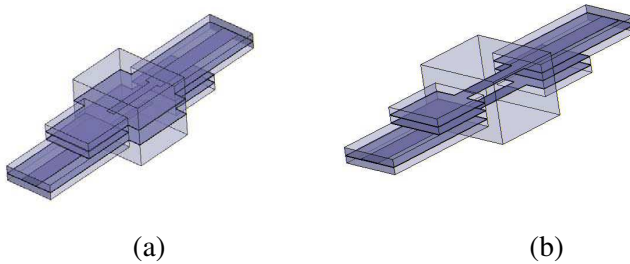

(a)   (b)

Figure 8. HFSS models of the vertical transition coupling structure using (a) full membrane and (b) reduced membrane lines.

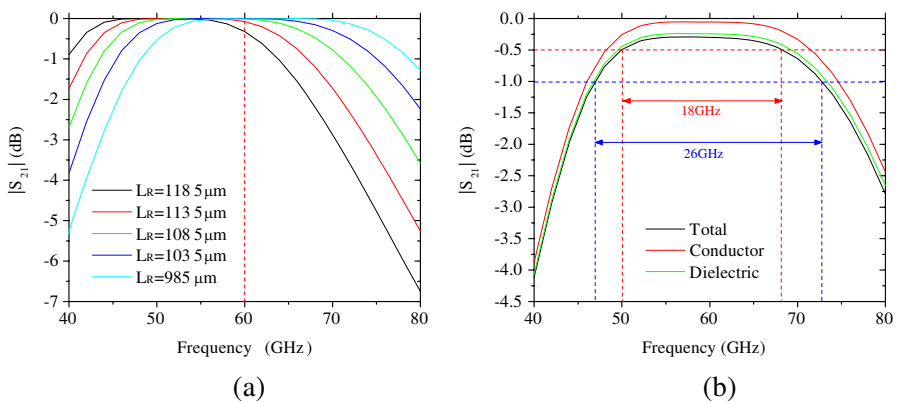(a)   (b)

Figure 9. Simulated results for the full membrane transition: (a) insertion loss over frequency, and (b) loss effects.

frequency.

The effect of loss on the modified structure's response was then investigated assuming gold conductors with zero surface roughness and a thickness of one micron, along with an SU-8 membrane. Figure 9(b) shows the major contribution to the loss of the structure is that of the dielectric with the ohmic loss being relatively small. However, the total loss of the structure is still extremely low with a loss of less than 1 dB over a 26 GHz bandwidth and 0.5 dB over 18 GHz. The addition of conductor surface roughness (40 nm on one side of the strip conductors and 10 nm on the shielding) to the simulation resulted in a loss increase of around 0.01 dB across the range. The simulated return loss for the structure is shown in Figure 10 and being greater than 14 dB across V-band was deemed to be acceptable.

As the majority of the insertion loss in the simulated structure is the dielectric loss of the thin membrane, it was thought a reduction in loss would be achieved through the removal of mechanically unimportant areas of the membrane as in the earlier work with transmission lines described in [1, 2]. The areas in which the membrane was removed can be seen in the HFSS model shown in Figure 10(b). The required length of the coupling region and strip width were calculated as $L = 1232\,\mu\text{m}$ and $W = 250\,\mu\text{m}$. Again, the length of the strip conductors in the coupling region needed to be reduced to achieve a centre frequency of 60 GHz and the optimum length was found to be $L_R = 1052\,\mu\text{m}$. A simulated S-parameter response can be seen in Figure 10 where a noticeable improvement in both the return
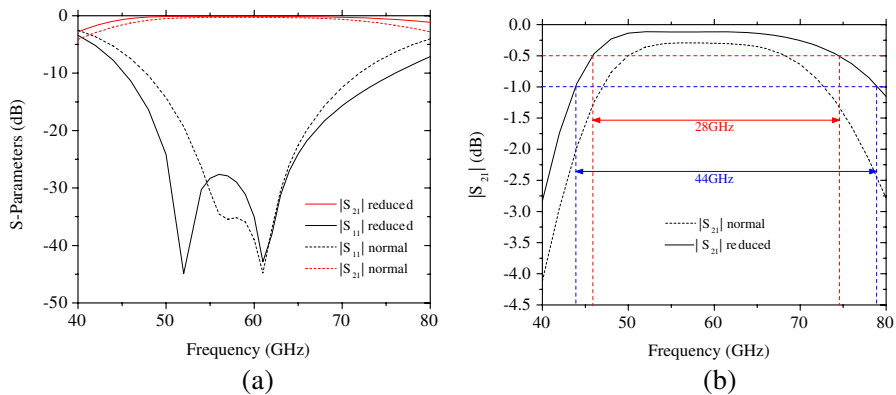

(a)   (b)

Figure 10. (a) Simulated S-Parameters plot comparing reduced membrane and normal coupling structures, and (b) comparison of $|S_{21}|$ for the normal and reduced membrane transitions.

and insertion loss is observed due to the reduction in membrane area. Here not only can a reduction in loss from 0.29 dB to 0.11 dB at 60 GHz be seen, but also a large increase in bandwidth (due to the reduced effective relative permittivity) with the 1 dB bandwidth increasing from 18 to 28 GHz and the 0.5 dB from 26 to 44 GHz. Incorporation of conductor surface roughness into the simulation (in the same manner as previously described) resulted again in a loss increase of around 0.01 dB. The performance is therefore comparable to the state of the art transitions discussed in Section 2.1.

4. CONCLUSION

The preliminary design concept for an electromagnetic coupling structure designed to act as a non-contact high-frequency transition between vertically adjacent levels of a 3D mm-wave MCM has been presented and initial design rules outlined This structure relies heavily on the versatility of the micromachining techniques used to locally vary the height of the shielding in the vicinity of the coupling region, and so allow the required level of coupling between two membrane-supported, fully-shielded lines. As such this is a key technology for the realization of a 3D membrane-based MCM. Due to its novel nature, this device needed to be extensively modelled to obtain the necessary design data. Once the electrical characteristics were defined in terms of the dimensional parameters, two versions of the transition were designed and simulated, with one using a reduced-membrane approach to minimise insertion loss. The results of these simulations showed performance better than that measured for state-of-the-art contact transitions, with insertion loss as low as 0.12 dB at 60 GHz for a structure with a 44 GHz 1 dB bandwidth.

The optimized vertical transition footprint is around 1.5 mm square with a depth of 1 mm at 60 GHz. This depth would be accommodated by the vertically adjacent lines (it is noted that this would place a design restriction on the positioning of vertical transitions on the vertically adjacent lines, and also the routing of the lines themselves). Although this footprint would be considered a large for a via in many MCM platform technologies, the proposed MCM technology is aimed at applications such as phased array systems and other high-performance high-frequency applications where minimization of loss is the most important factor which can be achieved at the cost of overall MCM size. Additionally a low degree of interconnected density is expected in such applications and so a relatively large via size can be tolerated.

It has also been ascertained from the modeling of this device, that

in addition to acting as a transition, various degrees of directional coupling can easily be achieved between adjacent levels in a 3D MCM. This would introduce an increased flexibility to a MCM designer and find many useful applications in circuits such as planar antenna array feed networks thereby offering an increase to the already high degree of functionality for any MCMs realized using this technology. A method of incorporating MMICs and other active devices in the proposed 3D MCM using membrane supported interconnect has also been outlined.

ACKNOWLEDGMENT

REFERENCES

1. Farrington, N. E. S. and S. Iezekiel, "Deisgn and simulation of membrane supported transmission lines for interconnects in a mm-wave multichip module," *Progress In Electromagnetics Research B*, Vol. 27, 165–186, 2011.

2. Farrington, N. E. S., "Micromachined transmission line interconnects for millimetre-wave multi-chip modules," Ph.D. thesis, School of Electrical and Electronic Engineering, The University of Leeds, 2005.

3. Dib, N. I., W. P. Harokopus, Jr., L. P. B. Katehi, C. C. Ling, and G. M. Rebeiz, "Study of a novel planar transmission line," *IEEE Int. Microwave Theory Tech. Symposium Digest*, 623–626.

4. Weller, T. M., G. M. Rebeiz, and L. P. Katehi, "Experimental results on microshield transmission line circuits," *IEEE MTT-S Digest*, 827–830, 1993.

5. Dib, N. I. and P. B. Katehi, "Impedance calculation for the microshield line," *IEEE Microwave and Guided Wave Letters*, Vol. 2, No. 10, 406–408, Oct. 1992.

6. Weller, T. M., L. P. Katehi, and G. M. Rebeiz, "High-performance microshield line components," *IEEE Trans. Microwave Theory Tech.*, Vol. 43, No. 3, 534–543, Mar. 1995.

7. Weller, T. M., L. P. Katehi, and G. M. Rebeiz, "A 250-GHz Microshield bandpas filter," *IEEE Microwave and Guided Wave Letters*, Vol. 5, No. 5, May 1995.

8. Petrini, I., F. Giacomozzi, D. Neculoiu, D. Vasilache, C. Buiculescu, and A. Muller, "Micromachined hybrid integrated

receiver modules for 38 GHz and 77 GHz, on silicon substrate, technology and manufacturing," *Semiconductor Conference, 2002, CAS 2002 Proc.*, Vol. 1, 29–32, Oct. 2002.

9. Duwe, K., S. Hirsch, and J. Muller, "Micromachined low pass filters and coplanar waveguides for D-band frequencies based on HMDSN-membranes," *MSMW 2001 Symposium Proc.*, 675–677, Jun. 2001.

10. Liu, W. Y., D. P. Steenson, and M. B. Steer, "Membrane-supported CPW with mounted active devices," *IEEE Microwave and Wireless Component Letters*, Vol. 11, No. 4, 167–169, Apr. 2001.

11. Liu, W. Y., "Mass produced copper-on-polymer-membrane boards for micromachined millimeter-wave circuits," *IEEE EDMO Proc.*, Vienna, 205–210, 2001.

12. Drayton, R. F. and L. P. B. Katehi, "Development of self-packaged high frequency circuits using micromachining techniques," *IEEE Trans. Microwave Theory Tech.*, Vol. 43, No. 9, 2073–2080, Sep. 1995.

13. Katehi, L. P. B. and G. M. Rebeiz, "Novel micromachined approaches to MMICs using low-parasitic, high-performance transmission media and environments," *IEEE Int. Microwave Theory Tech. Symposium Digest*, 1145–1148, 1996.

14. Robertson, S. V., L. P. B. Katehi, and G. M. Rebeiz, "Micromachined W-band filters," *IEEE Trans. Microwave Theory Tech.*, Vol. 44, No. 4, 598–606, Apr. 1996.

15. Rebeiz, G. M., L. P. B. Katehi, T. M. Weller, C. Y. Chi, and S. V. Robertson, "Micromachined membrane filters for microwave and millimetre-wave applications (Invited article)," *Int. J. of Microwave and Millimeter-wave Computer Aided Engineering*, Vol. 7, 149–166, Feb. 1997.

16. Robertson, S. V., A. R. Brown, L. P. B. Katehi, and G. M. Rebeiz, "A 10-60-GHz micromachined directional coupler," *IEEE Trans. Microwave Theory Tech.*, Vol. 46, No. 11, 1845–1849, Nov. 1998.

17. Henderson, R. M., T. M. Weller, and L. P. B. Katehi, "Three-dimensional W-band circuits using Si micromachining," *IEEE Int. Microwave Theory Tech. Symposium Dig.*, Vol. 2, 13–19, 441–444, Jun. 1999.

18. Lee, K. Y., N. LaBianca, S. A. Rishton, S. Zolgharnain, J. D. Gelorme, J. Shaw, and T. H. P. Chang, "Micromachining applications of a high resolution ultrathick photoresist," *J. Vacuum Science and Technology B.*, Vol. 13, No. 6, 3012–3016, Nov./Dec. 1995.

19. Lorenz, H., M. Despont, N. Fahrni, N. LaBianca, P. Renaud, and P. Vettiger, "SU-8: A low-cost negative resist for MEMS," *J. of Micromechanical Microengineering*, Vol. 7, 121–124, 1997.

20. Despont, M., H. Lorenz, N. Fahrni, J. Brugger, P. Renaud, and P. Vettiger, "High-aspect-ratio, ultrathick, negative-tone near-UV photoresist for MEMs applications," *IEEE Proc. Int. Workshop on Micro-electro Mechanical Systems*, 518–522, Jan. 1997.

21. Lorenz, H., M. Laudon, and P. Renaud, "Mechanical characterization of a new high-aspect_ratio near UV-photoresist," *J. Microelectronic Engineering*, Vol. 41–42, 371–374, 1998.

22. Farrington, N. E. S. and S. Iezekiel, "Accurate layer thickness control and planarization for multi-layer SU-8 structures," *SPIE J. Micro./Nanolith. MEMS MOEMS*, Vol. 10, 013019, Mar. 29, 2011, doi:10.1117/1.3563599.

23. Henderson, R. M., K. J. Herrick, T. M. Weller, S. V. Robertson, R. T. Kihm, and L. P. B. Katehi, "Three-dimensional high-frequency distribution networks. II. Packaging and integration," *IEEE Trans. Microwave Theory Tech.*, Vol. 48, No. 10, 1643–1651, Oct. 2000.

24. Katehi, L. P. B., J. F. Harvey, and K. J. Herrick, "3-D integration of RF circuits using Si micromachining," *IEEE Microwave Magazine*, 30–39, Mar. 2001.

25. Coutant, M. and K. Chang, "Broadband, electrically long vertical waveguide interconnect," *Electronic Letters*, Vol. 36, No. 25, 2076–2078, Dec. 2000.

26. Davidovitz, M., R. A. Sainati, and S. J. Fraasch, "A non-contact interconnect through an electrically thick ground plate common to two microstrip lines," *IEEE Trans. Microwave Theory Tech.*, Vol. 43, No. 4, 753–759, Apr. 1995.

27. Jackson, R. W. and D. W. Matolak, "Surface-to-surface transition via electromagnetic coupling of coplanar waveguides," *IEEE Trans. Microwave Theory Tech.*, Vol. 35, No. 11, 1027–1031, Nov. 1987.

28. Ho, C.-H., L. Fan, and K. Chang, "Slot-coupled double-sided microstrip interconnects and couplers," *IEEE Int. Microwave Theory Tech. Symposium Digest*, 1321–1324, Jun. 1993.

29. VandenBerg, N. L. and L. P. B. Katehi, "Broadband vertical interconnects using slot-coupled shielded microstrip lines," *IEEE Trans. Microwave Theory Tech.*, Vol. 40, No. 1, 81–88, Jan. 1992.

30. Raskin, J.-P., G. Gauthier, L. P. B. Katehi, and G. M. Rebeiz, "W-band single-layer vertical transitions," *IEEE Trans. Mi-*

crowave Theory Tech., Vol. 48, No. 1, 161–164, Jan. 2000.

31. Herrick, K. J., J.-G. Yook, and L. P. B. Katehi, "Microtechnology in the development of three-dimensional circuits," *IEEE Trans. Microwave Theory Tech.*, Vol. 46, No. 11, 1832–1844, Nov. 1998.

32. Ommodt, K., S. Sanzgiri, F. German, and T. Jones, "Vertical interconnects for phased array packaging," *IEEE Antennas and Propagation Society Int. Symposium Dig.*, Vol. 2, 1334–1337, Jul. 1996.

33. Minotani, T., Y. Royter, H. Ishii, A. Hirata, K. Machida, A. Sasaki, and T. Nagatsuma, "Three-dimensional millimeter-wave photonic integrated circuits on Si," *IEEE Int. Microwave Theory Tech. Symposium Dig.*, Vol. 1, 57–60, May 2001.

34. Goverdhanam, K., R. N. Simons, and L. P. B. Katehi, "Novel three-dimensional vertical interconnect technology for microwave and RF applications," *IEEE Int. Microwave Theory Tech. Symposium Dig.*, Vol. 2. 641–644, Jun. 1999.

35. Becker, J. P. and L. P. B. Katehi, "Multilevel finite ground coplanar line transitions for high-density packaging using silicon micromachining," *IEEE Int. Microwave Theory Tech. Symposium Dig.*, Vol. 1, 303–306, Jun. 2000.

36. Alléaume, P., C. Toussain, T. Huet, and M. Camiade, "Millimeter-wave SMT low cost plastic packages for automotive RADAR at 77 GHz and high data rate E-band radios," *IEEE Int. Microwave Theory Tech. Symposium Dig.*, Vol. 1, 789–792, Jun. 2009.

37. Byun, W., B. Kim, K. Kim, K. Eun, M. S. Kulke, R. Kersten, O. Mollenbeck, G. Rittweger, and M. Daejeon, "Design of vertical transition for 40 GHz transceiver module using LTCC technology," *Proc. European Microwave Integrated Circuit Conference, EuMIC 2007*, 555–558, Munich, Germany, 2007.

38. Lau, J. H., "Flip chip technologies," *McGraw Hill*, 1996.

39. Lin, J.-K., J. Drye, W. Lytle, T. Scharr, R. Subrahmanya, and R. Sharma, "Conductive polymer bump interconnects," *IEEE Proc. Electronic Components and Technology Conference*, 1059–1068, May 1996.

40. Oh, K. W. and C. H. Ahn, "Flip-chip packaging with micromachined conductive polymer bumps," *IEEE Proc. Adhesive Joining and Coating Technology in Electronic Manufacturing*, 224–228, Sep. 1998.

41. Oh, K. W., C. H. Ahn, and K. P. Roenker, "Flip-chip packaging using micromachined conductive polymer bumps and alignment pedestals for MOEMS," *IEEE J. on Selected Topics in Quantum*

Electronics, Vol. 5, No. 1, 119–126, Jan./Feb. 1999.

42. Oh, K. W. and C. H. Ahn, "A new flip-chip bonding technique using micromachined conductive polymer bumps," *IEEE Trans. Advanced Packaging*, Vol. 22, No. 4, 586–591, Nov. 1999.

43. Li, C., F. E. Sauser, R. Azizkhan, C. H. Ahn, and I. Papautsky, "Polymer flip-chip bonding of pressure sensors on flexible kapton film for neonatal catheters," *IEEE Int. Conf. Proc., Micro Electro Mechanical Systems, MEMS*, 749–752, 2004.

44. Pozar, D. M., *Microwave Engineering*, 2nd edition, John Wiley and Sons Inc., 1998.

45. Matthaei, G. L., L. Young, and E. M. T. Jones, *Microwave Filters, Impedance-matching Networks, and Coupling Structures*, Artech House, 1980.